Journal of Materials Chemistry C

ROYAL SOCIETY OF CHEMISTRY

COMMUNICATION

View Article Online
View Journal



Cite this: DOI: 10.1039/d5tc03932k

Received 4th November 2025,
Accepted 22nd January 2026

DOI: 10.1039/d5tc03932k

rsc.li/materials-c



# Controlling self-assembly and charge transport in photo-responsive nanostructured materials

Yu Cao, *[ab] Tejal Nirgude,[c] Frédéric Dubois,[d] Dharmendra Pratap Singh, *[d] Fengcheng Xi,[a] Feng Liu [ab] and Mohamed Alaasar *[ce]

**We report a new class of photo-responsive polar nanostructured liquid crystals. Controlled aromatic core fluorination directs self-assembly into a novel tetragonal mesophase with co-existing columns and micelles. These unique nanostructured materials enable tunable charge transport, providing a design model for functional organic semiconductors.**

## Introduction

The design and development of advanced functional materials with tailored properties have become a cornerstone of modern materials science.[1] Among these, π-conjugated liquid crystals (LCs) have emerged as versatile platforms for a wide range of technological applications such as electronic, optical, light harvesting[2] and photonic applications[3,4] due to their unique combination of order and mobility. Particularly, extended π-conjugated polycatenar (multichain) LCs represent an important class of self-assembling materials that exhibit fascinating structural and functional properties.[5,6] They are known for their potential electronic applications, including organic light-emitting diodes (OLEDs),[7,8] organic field-effect transistors (OFETs),[9,10] and organic photovoltaics (OPVs).[11,12] The key role of effective operations of these devices depends on their charge-transporting abilities.[5] Most of the polycatenars used for such applications have symmetrical multiple flexible terminal chains attached to the rigid core, which results in most cases in columnar phases.[5,12–17]

[a] Shaanxi International Research Center for Soft Matter, State Key Laboratory for Mechanical Behavior of Materials, Xi'an Jiaotong University, Xi'an, P. R. China
[b] Institute of New Concept Sensors and Molecular Materials, Shaanxi Key Laboratory of New Concept Sensors and Molecular Materials, Xi'an Jiaotong University, Xi'an 710049, P. R. China
[c] Institute of Chemistry, Martin Luther University Halle-Wittenberg, 06120 Halle Saale, Germany. E-mail: mohamed.alaasar@chemie.uni-halle.de
[d] UDSMM, Unité de Dynamique et Structure des Matériaux Moléculaires, Université du Littoral Côte d'Opale, UR 4476, Calais F-62228, France
[e] Chemistry Department, Faculty of Science, Cairo University, 12613 Giza, Egypt. E-mail: malaasar@sci.cu.edu.eg

Another interesting class of polycatenar LCs is rod-like molecules having the terminal chains unequally distributed at both termini of the aromatic backbone, which have recently attracted significant attention due to their ability to self-assemble into mesophases with three-dimensional architectures.[18] The lack of molecular symmetry acts to intensify the defining features of the local aromatic backbone. Therefore, these achiral nonsymmetric polycatenars were able to display chiral isotropic liquid phases assigned as $Iso_1^{[*]}$ phases as well as chiral and achiral bicontinuous cubic phases composed of helical networks.[19–21] Polycatenars featuring a polar aromatic core could exhibit semiconducting behaviour in their liquid crystalline states, making them attractive candidates for ultrafast light switching and non-volatile data storage.

The incorporation of specific functional groups and structural elements in LCs can dramatically influence their self-assembly behaviour and physical properties. Recent studies have demonstrated that the introduction of heterocyclic units such as [1]benzothieno[3,2-*b*]benzothiophene (BTBT) or bithiophene in non-symmetric rod-like polycatenars can lead to materials with enhanced thermal stability, improved mesophase ranges, and potential electronic applications.[22–24] Introducing the azobenzene unit was also successful in inducing transition between chiral and achiral LC phases as a result of *trans–cis* photoisomerization under light irradiation.[25] The number of reported hockey-stick polycatenars is very limited, incorporating 2,5-disubstituted thiophene,[26] 4-cyanoresorcinol[27,28] or 1,3,4-oxadiazole[29] as central bent-core units. In the latter case, hexagonal columnar phases were observed, which become ferroelectric by introducing one or two fluorine atoms in their molecular structures.[25]

Herein, we introduce 4-bromoresorcinol as a new building block for designing novel nanostructured self-assembled functional nonsymmetric hockey-stick (HS) polycatenars (**AHH**, **AFH**, and **AFF**, Scheme 1). The new molecular design combines the photoresponsive properties of the azobenzene unit and the possibility of modifying the molecular packing, π-stacking behaviour, and electronic properties by using the bromine substitution at the apex of the bent-core structure, as well as aromatic core fluorination at different positions.

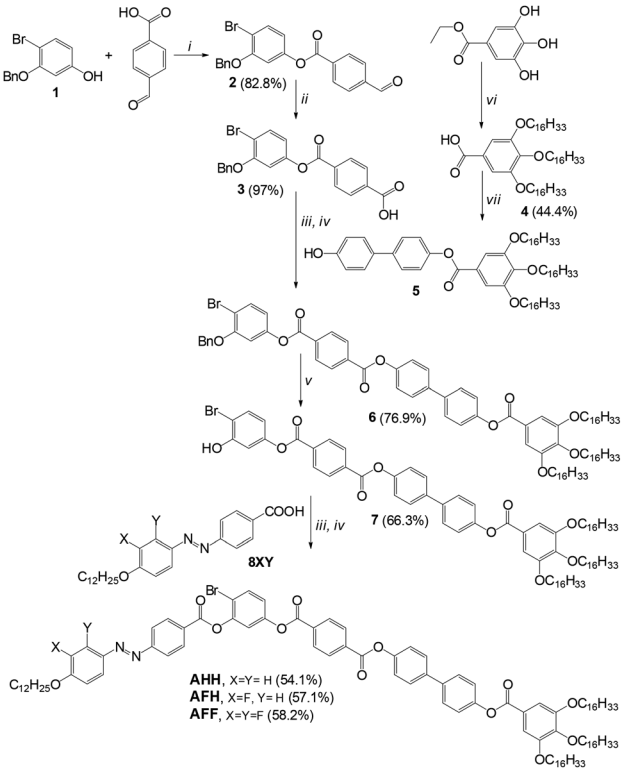


Scheme 1 Synthesis of the target HS polycatenars **AH**, **AHF**, and **AFF**. Reagents and conditions: (i) DCC, DMAP, dry $CH_2Cl_2$, stirring 24 h; (ii) $NaOCl_2$, $Na_2HPO_4$, resorcinol, *tert*-butanol, stirring overnight; (iii) DMF, $SOCl_2$, reflux 1 h; (iv) dry $CH_2Cl_2$, dry TEA, dry pyridine, reflux for 6 h; (v) $H_2$, Pd/C-10%, dry THF, stirring 24 h; (vi) (1) $BrC_{16}H_{33}$, $K_2CO_3$, KI, 2-butanone; (2) hydrolysis, acidification; (vii) (1) DMF, $SOCl_2$, reflux 1 h; 4,4′-dihydroxybiphenyl, pyridine, stirring overnight.

The position of fluorine substitution not only influences the polar characteristics of the mesophase but also alters its range and type, where columnar and a novel type of tetragonal LC phase are observed for the new materials. Moreover, the LC phases display polar characteristics and hole mobility in the range of $10^{-2}$–$10^{-5}$ $cm^2\ V^{-1}\ s^{-1}$ as measured by the space charge limited current (SCLC) technique. Therefore, our findings establish new design principles for nanostructured organic semiconductors and provide a novel self-assembly pathway connecting columnar and micellar phases.

## Results and discussion

### Synthesis and characterization

The synthesis of the new HS polycatenars **AHH**, **AFH**, and **AFF** is shown in Scheme 1. All synthesis details and analytical data of the intermediates and final compounds are given in the SI. Each compound of the new materials exhibits one type of mesophase as indicated by the DSC heating and cooling cycles. As can be seen from the DSC traces (Fig. S9–S11), the LC phases are enantiotropic in all cases, with a range that is strongly dependent on the degree of aromatic core fluorination. Therefore, the mesophase range of the nonfluorinated compound

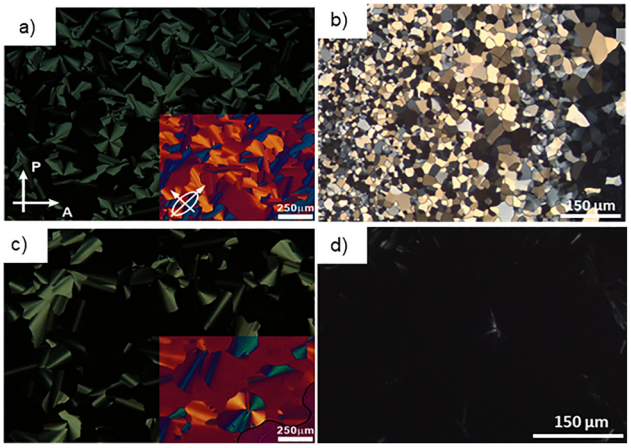


Fig. 1 Optical textures observed on cooling from the isotropic liquid phase under crossed polarizers for: (a) columnar phase of **AHH** at 100 °C; (b) tetragonal phase of **AFH** at 95 °C; (c) columnar phase of **AFF** at 95 °C and (d) columnar phase of **AFF** at 95 °C after cooling from the temperature above the clearing temperature under a 5 V $\mu m^{-1}$ electric field showing the perfect alignment of the mesophase. The direction of the polarizers in all cases is given in (a).

(**AHH**, Fig. S9) is almost the same for the double-fluorinated one (**AFF**, Fig. S11), while the monofluorinated (**AFH**, Fig. S10) material exhibits a narrower mesophase range. Under the polarized optical microscope (POM), the materials show the textures observed in Fig. 1. For the nonfluorinated material **AHH**, a spherulitic texture is observed at the transition from the isotropic liquid phase for the whole range of the mesophase till the start of the crystallization. All transitions, *i.e.*, Iso-LC and LC-Cr, either on cooling or heating, could also be detected during DSC investigations (Fig. S9). The same also applies to the other two materials (Fig. S10 and S11). For the monofluorinated compound **AFH**, a characteristic mosaic-like texture could be seen (Fig. 1b), while for the double-fluorinated material, a different texture is observed (Fig. 1c). Interestingly, all LC phases for all three compounds could be perfectly aligned on cooling from the isotropic liquid state under an electric field (*e.g.*, compare Fig. 1c and d), which is important for applications.

To investigate the LC phases exhibited by the new materials, we performed SAXS investigations and reconstructed the electron density (ED) maps. For **AHH**, the SAXS pattern exhibits three sharp peaks, suggesting a highly ordered LC phase (Fig. 2a). The phase can be indexed as a *p6mm* hexagonal columnar phase, as the position of the three peaks shows a typical ratio of $1:\sqrt{3}:2$. Such a phase is also in line with the POM observation in Fig. 1a. The lattice parameter of the 2D hexagonal phase is 5.27 nm. Calculated from the lattice volume and molecular volume (Table S1), about 5 molecules form a raft in each column. The reconstructed ED map shows that the columns in the lattice have circular cross-section and a uniform low ED region (Fig. 2b), suggesting the free rotation of molecular rafts. However, measured from the ED map, the high ED region is ~3.1 nm, which is in line with the aromatic core size (~3.1 nm) refined by the DFT calculation (Fig. S16). Such similarity suggests molecular rafts are perpendicular to the columnar axis, which is also

 

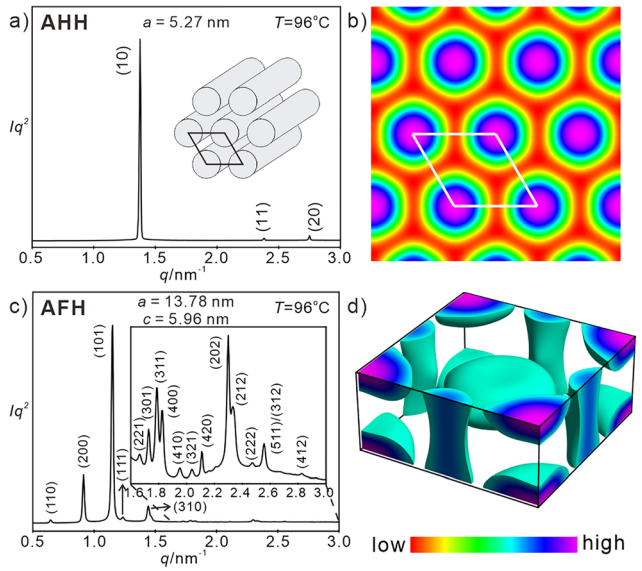


Fig. 2 (a) The SAXS diffractogram of **AHH** referring to the hexagonal columnar phase at 96 °C; (b) the reconstructed ED map of *p6mm* phase with white lines indicating the lattice; (c) the SAXS diffractogram of **AFH** referring tthe tetragonal $P4_2/mnm$ phase at 96 °C; (d) the reconstructed ED map of the $P4_2/mnm$ phase containing both micelles and columns. Purple indicates high ED, while red indicates low ED. For detailed data, see Tables S1–S3.

supported by the POM texture with λ-plate (Fig. 1a). Inserting the retarder induces the blue colour in the northeast-southwest direction, a typical result for optically negative spherulites, suggesting the high index axis is radial. Since the columns are tangential in the fans, it follows that the bent-cores are perpendicular to the columns. The introduction of two fluorine atoms at one terminal of the aromatic core in **AFF** does not alter the mesophase type compared to the non-fluorinated **AHH** (Fig. 1c and Fig. S12). Even the lattice parameters are almost the same (Tables S1 and S3).

Interestingly, the monofluorinated alternative, **AFH**, exhibits a totally different SAXS pattern (Fig. 2c). The complex pattern can be indexed as a tetragonal phase with the $P4_2/mnm$ space group (Fig. S13). The tetragonal phase is also supported by the POM mosaic texture. Surprisingly, the tetragonal lattice is extremely large, with $a$ = 13.78 nm and $c$ = 5.96 nm, containing ∼546 molecules (Tables S2 and S4). The reconstructed ED map suggests the phase is a body-centered tetragonal phase consisting of large micelles at the center/corner and columns along the $c$ direction (Fig. 2d and Fig. S14). Measured from the ED map, the radius of the micelle is ∼4.5 nm and the height of the micelle is ∼3.0 nm, which suggests that micelles are formed by a large bundle of molecules along $c$ direction. The average cross-section of aromatic core and alkyl chains is normally ∼0.3 nm$^2$,[30] *i.e.*, two micelles are composed of ∼424 molecules. In this way, each column contains about 13 layers of molecular raft based on the WAXS diffractograms (Fig. S15), and each raft contains about 5 molecules, like the columnar phase of **AHH** and **AFF**.

The special phase sequence upon aromatic core fluorination *p6mm* (**AHH**) – $P4_2/mnm$ (**AFH**) – *p6mm* (**AFF**) can be attributed to the volume expansion induced by fluorine atoms substituted at different positions. The effect of fluorination on both polar interaction and steric effect is well known.[31,32] The significant steric volume effect of fluorine, when positioned near the alkyl chains, promotes a transition from a columnar to a micellar phase by increasing the interfacial curvature.[19,25,33] In the current case, fluorination significantly influences the molecular packing according to the WAXS (Fig. S15). For **AFH**, polar interactions between fluorinated and non-fluorinated benzene rings shrink the intermolecular distance and π–π stacking distance (Fig. S15b and e) compared with **AHH** (Fig. S15a and d). Such an effect, combined with the volume of the fluorine atom close to the alkyl chain, disturbs the volume ratio between aromatic and aliphatic regions. This frustration results in a phase comprising a mixture of columns and micelles, which exhibits reduced thermal stability and a narrower phase range compared to the hexagonal phase formed by **AHH**. On the other hand, the additional inner fluorine in **AFF** shows more steric effect as part of the aromatic core, leading to an expansion of intermolecular distance (Fig. S15c and f). Thus, inner fluorination expands the volume of the aromatic core simultaneously, reforming the columnar phase with hexagonal symmetry. Therefore, the degree and position of fluorination induce subtle volume change, transforming the self-assembled phase between the conventional columnar phase and an intermediate tetragonal phase ($P4_2/mnm$), combining both columns and micelles. It's worth noting that such an intermediate phase provides a new routine for the columnar to micellar phase transition, which is commonly found for soft self-assembly related to controlled photo behaviour, energy application, and biomaterials.[34,35] The distinct phase sequence observed—*p6mm* for **AHH**, $P4_2/mnm$ for **AFH**, and *p6mm* for **AFF**—directly correlates with charge-transport behaviour. In **AHH** and **AFF**, the continuous hexagonal columnar phases provide ordered, one-dimensional stacks of overlapping aromatic π-systems along the column axes, facilitating efficient hole-carrier pathways. Conversely, the mixed column–micelle architecture in the tetragonal phase of **AFH** introduces torturous hopping barriers and structural discontinuities that significantly reduce charge-transport efficiency. This structure–function relationship illustrates how controlled aromatic fluorination tunes both self-assembly and semiconductor performance through subtle modulation of intermolecular packing geometry. To further confirm the molecular packing and dynamics in the special phases due to core-fluorination, we preliminarily investigated the dielectric response of the compounds. The tan $\delta$ curves of the compounds **AHH**, **AFH**, and **AFF** are plotted in Fig. 3.

In the Col phase (80–100 °C), compound **AHH** didn't display a distinct relaxation mode, which is possibly out of the test range due to the best mobility as LC; however, compound **AFH** exhibited a strong relaxation mode (*i.e.*, α-relaxation) around $10^4$ Hz, which is attributed to the collective rotations of bent-core molecules in the micelles, similar to smectic phase in-plane rotation. This relaxation is assigned to be the α-relaxation due to its strong temperature dependence, which critically describes how molecules reorient under external fields and

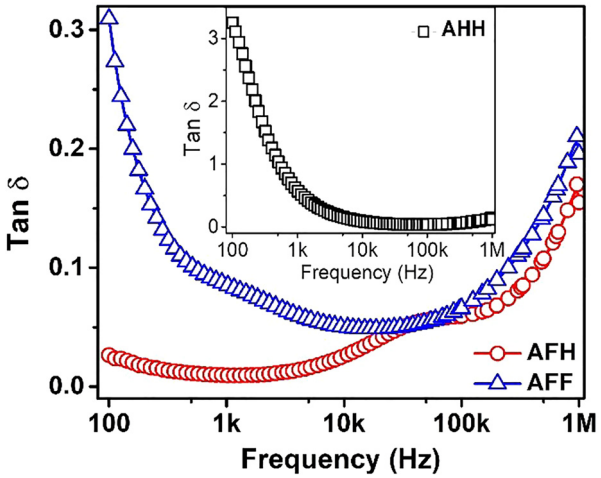


Fig. 3 The variation of Tan $\delta$ as a function of frequency for the compounds **AHH**, **AFH**, and **AFF**. The dielectric investigation was carried out in the 9 μm-thick cells.

provides information about the intermolecular interactions and phase structure.[36] In the **AFH** compounds, the molecules form micelles, with a minor tilt that allows them to conform to the lattice, so facilitating molecular fluctuations. For **AFF** in which F-atom substitution is made at X- and Y-positions, the relaxation mode weakens and is also shifted to a lower frequency around 1 kHz. Such a shift can be due to the freezing of molecules during crystallization, supported by the extra sharp peaks in WAXS (Fig. S15). The dielectric investigation of these compounds requires a detailed investigation and is subject to a separate study, which will be presented in the near future.

### Charge transport properties

The bent-core architecture, LC phase types, and photo-responsive nature (see Fig. S18) of the new materials render them as promising candidates for electronic applications requiring extraordinary alignment. The charge transport properties and subsequently the determination of hole mobility for the **AHH**, **AFH**, and **AFF** compounds were carried out using the space charge limited current (SCLC) technique.[37–39] Charge transfer in these polycatenars mostly occurs *via* the π-conjugated aromatic backbone, particularly the bent-core structure connecting the azobenzene and resorcinol units, which constitutes the high-electron-density areas inside the columns or micelles. The adaptable alkyl chains function mainly as insulating spacers that delineate low electron density areas and provide interfacial curvature, yet do not directly engage in hole transport. Exhibiting multiple phenyl rings, azo linkage, carboxylate group, and long alkoxy side chains, **AHH**, **AFH**, and **AFF** are classically electron-rich compounds. All compounds show high HOMO energy levels and render an efficient hole transport nature. Therefore, the hole-only devices consisting of Glass/ITO/LC/Au were constructed by maintaining the thickness of the devices ≈ at 9 μm (Fig. S19). In the SCLC technique, the charges are injected by Au electrodes and are drifted towards another electrode (*i.e.*, ITO), propagating through the LC material. Thus, the obtained current density is associated with the mobility

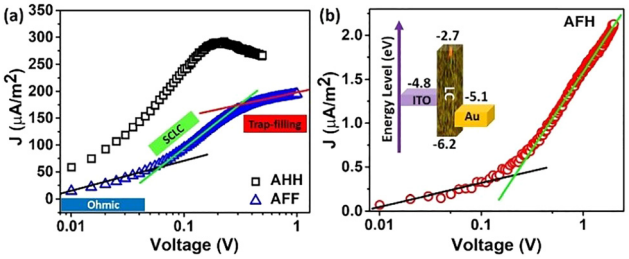


Fig. 4 Current density (*J*) *vs.* voltage (*V*) curves for the (a) **AHH**, **AFF**, and (b) **AFH** at 100 °C. The inset of (b) represents the arrangement of energy levels in the hole-only SCLC device.

of charge carriers, and the mobility value can be determined by the Mott–Gurney equation ($J = 9\varepsilon_0\varepsilon\mu V^2/8d^3$) by assuming the negligible contribution of traps. At 100 °C, *J*–*V* curves were plotted to determine the hole mobility values for **AHH**, **AFH**, and **AFF** in the different LC phases as depicted in Fig. 4.

It has been observed that the **AHH** compound exhibits the highest current density, whereas the **AFH** compound shows the lowest. The estimated mobility values are tabulated in Table 1.

For the **AHH** compound, the highest hole mobility of $2.68 \times 10^{-2}$ cm$^2$ V$^{-1}$ s$^{-1}$ at 100 °C has been noticed, attributed to the best π-electron delocalization and least carrier localization. When a fluorine atom is substituted at the X and Y-positions (**AFF**), a strong inductive effect comes into existence, which results in an increased energetic disorder and reduces the hole mobility. Therefore, in the double fluorinated compound **AFF**, hole mobility of $2.65 \times 10^{-3}$ cm$^2$ V$^{-1}$ s$^{-1}$ was observed. This high value of hole mobility ($\approx 10^{-2}$–$10^{-3}$ cm$^2$ V$^{-1}$ s$^{-1}$) is in good agreement with that of the recently reported value for calamitic sterol-based calamitic ionic LC material.[38] It should be noted that the non-fluorinated **AHH** and difluorinated **AFF** compounds constitute a hexagonal columnar phase exhibiting almost the same lattice parameters (≈5.4 nm). On the other hand, in the **AFH** compound, a mono fluorination introduces localization of charges and forms a novel tetragonal $P4_2/mnm$ phase combining both columns and micelles. **AFH** compound showed the least hole mobility compared to **AHH** and **AFF**, probably due to the formation of mixed tetragonal $P4_2/mnm$ phase in which charges are trapped between the boundaries of the columns and micelles, resulting in a large reduction in conduction current. As the SCLC mobility primarily depends upon the conduction current in the space-charge region, as a result, we observed the lowest hole mobility ($2.48 \times 10^{-5}$ cm$^2$ V$^{-1}$ s$^{-1}$) for the **AFH** compound due to the least effective charge-transport pathways. Conclusively, the observed order of hole mobility in the **AHH**, **AFF**, and **AFH**

Table 1 Comparison of hole mobility and polarization recorded at 100 °C in the cooling cycle. Polarization was recorded by applying a frequency of 60 Hz and a field of 10 V μm$^{-1}$

| Comp. | Hole mobility (cm$^2$ V$^{-1}$ s$^{-1}$) | Polarization (nC cm$^{-2}$) |
|---|---|---|
| **AHH** | $2.68 \times 10^{-2}$ | 77.56 |
| **AFF** | $2.65 \times 10^{-3}$ | 54.97 |
| **AFH** | $2.48 \times 10^{-5}$ | 66.68 |

compounds is as follows: $\mu_{AHH} > \mu_{AFF} > \mu_{AFH}$. Such a trend is in line with the HOMO/LUMO analysis (Fig. S17). HOMO concentrates on the non-fluorinated wings, and LUMO is on the fluorinated wings. In line with the ESP distribution and volume effect, the hockey-stick molecules would pack into anti-parallel ways, which creates overlap of HOMO and LUMO. The alternating HOMO and LUMO enhances the conductivity. The energy band alignment influences the performance of SCLC devices, as the recorded current density of charge carriers is directly proportional to their mobility. We determined the frontier orbital energies (HOMO and LUMO levels) of **AHH**, **AFH**, and **AFF** and DFT calculations (see Figures S16 and S17 in SI). As per simulation results, the HOMO energy level of the compounds is $\approx -6.2$ eV; therefore, the ITO–HOMO barrier and Au–HOMO barrier is $\approx 1.4$ and $\approx 1$ eV, respectively, representing that the electron-only transport is suppressed and hole migration is only allowed. Fig. 4 clearly indicates that the **AFF** compound demonstrates a nearly trap-free SCLC (slope $\approx$ 2), while compound **AHH** displays a trap-controlled SCLC characteristic. Consequently, the results are deemed acceptable according to the Mott–Gurney model; yet, the potential for mistake persists in the calculated values of hole mobilities.

### Polarization studies

To understand the origin of high hole mobility, we first focused on the polarization properties of all compounds. To the best of our knowledge, up to date, there is only one report about polar columnar phases exhibited by hockey-stick polycatenars.[29] Given that **AHH**, **AFH**, and **AFF** constitute a new class of hockey-stick polycatenars, we investigated their inherent polarization using the polarization current reversal method (Fig. S20).[40] Compound **AHH** exhibited a polarization value of 77.56 nC cm$^{-2}$ under the application of a DC electric field of 10 V μm$^{-1}$. The fluorine (F-atom) substitution causes the change in liquid crystal lattice parameters due to strong inductive effects. This results in a decrease in polarization value for the **AFH** compound, which is 66.68 nC cm$^{-2}$ at 10 V μm$^{-1}$. The steric hindrance produced by the F-substitution requires a larger applied field for switching the liquid crystal molecules. Further fluorination (F-atom substitution at the X- and Y-positions) reduces the electron density in the core due to steric hindrance (see also the ED map in Fig. 2d), which dominates over the strong polar inductive effects and results in a net decrease in the polarization value.[29] For compound **AFF**, the polarization value was noticed to be 54.97 nC cm$^{-2}$ at 10 V μm$^{-1}$ (Table 1).

The molecular structures of **AHH**, **AFH**, and **AFF** contain distinct functional groups that collectively govern self-assembly and charge transport. The bromine substituent at the apex of the bent-core unit modulates the local dipole moment and polar interactions, influencing molecular packing within the mesophase. The azobenzene unit extends π-conjugation along the aromatic backbone, contributing to frontier orbital delocalization and supporting hole transport along the columnar stacks; additionally, it imparts photo-responsiveness (demonstrated in Fig. S18). In the present device (Fig. S19), these groups function primarily to tune self-assembly and electronic structure rather than to serve as isolated charge-transport centers, and photo-switchable transport, which will be the subject of future detailed study.

Considering the distinct phase types in the three compounds, we would say that the hole mobility is governed by a complex interplay of molecular polarity, supramolecular architecture, and charge transport pathways. In the case of **AFH**, the presence of discontinuous micellar domains within its tetragonal phase severely disrupts these pathways, leading to a marked reduction in mobility and underscoring the dominant influence of the supramolecular self-assembly. For differences between **AHH** and **AFF** with the same hexagonal columnar phase, the polarity and mobility help **AHH** form a more ordered phase. From the DFT simulation (Fig. S16), **AHH** supports the anti-parallel packing better from the perspective of electron distribution, which leads to dense packing in each molecular raft and boosts hole mobility. On the contrary, WAXS suggests that **AFF** slightly crystallizes (Fig. S15).

## Conclusions

In summary, we have reported the design and synthesis of a new class of nanostructured functional hockey-stick polycatenar liquid crystalline materials exhibiting polar properties. We demonstrate that systematic fluorination of the aromatic core is a powerful tool for controlling self-assembly and charge transport properties. Specifically, steric effects from monofluorination induce a novel tetragonal LC phase in the case of **AFH** that combines columnar and micellar morphologies. This structural transition directly governs the materials' functional properties, enhancing both conductivity and macroscopic polarity. Furthermore, the incorporation of azobenzene units grants photo-responsive behaviour, positioning these new functional LCs as promising candidates for advanced electro-optic applications. Moreover, this work establishes key molecular design principles for engineering polar order in soft matter.

## Author contributions

Y. C. and M. A. conceived the project and supervised the research. T. N. and M. A. performed the synthesis and microscopic investigations, D. P. S. performed the charge transport and polarization measurements, Y. C. conducted the SAXS investigations, F. D. performed the dielectric measurements, F. X. and F. L. participated in some of the experiments and the data analysis, M. A., Y. C., D. P. S. drafted and revised the manuscript.

## Conflicts of interest

There are no conflicts to declare.

## Data availability

The data supporting this article have been included as part of the supplementary information (SI). Supplementary information: methods; synthesis of the final materials; NMR spectra;

DSC thermograms; SAXS data; DFT data; photoisomerization; charge transport studies *via* space charge limited current (SCLC) technique; polarization measurements. See DOI: https://doi.org/10.1039/d5tc03932k.

## Acknowledgements

M. Alaasar acknowledges the German Research Foundation (DFG) for the financial support (AL2378/1-2 and 424355983). Y. Cao acknowledges the National Natural Science Foundation of China (No. 12204369, 22572151). We thank the Shanghai Synchrotron Radiation Facility of BL16B1 (https://cstr.cn/31124.02. SSRF.BL16B1) for assistance on SAXS measurements.

## Notes and references

1 T. Kato, M. Yoshio, T. Ichikawa, B. Soberats, H. Ohno and M. Funahashi, *Nat. Rev. Mater.*, 2017, **2**, 17001.
2 M. Hecht and F. Würthner, *Acc. Chem. Res.*, 2021, **54**, 642.
3 R. K. Gupta and A. A. Sudhakar, *Langmuir*, 2019, **35**, 2455.
4 Z.-G. Zheng, Y.-Q. Lu and Q. Li, *Adv. Mater.*, 2020, **32**, 1905318.
5 R. De and S. K. Pal, *Chem. Commun.*, 2023, **59**, 3050.
6 R. De, S. Sharma, S. Sengupta and S. K. Pal, *Chem. Rec.*, 2022, **22**, e202200056.
7 C. Keum, D. Becker, E. Archer, H. Bock, H. Kitzerow, M. Gather and C. Murawski, *Adv. Opt. Mater.*, 2020, **8**, 2000414.
8 M. Funahashi and Y. Mori, *Mater. Chem. Front.*, 2020, **4**, 2137.
9 H. Iino, T. Usui and J. Hanna, *Nat. Commun.*, 2015, **6**, 6828.
10 D. H. Kim, B.-L. Lee, H. Moon, H. M. Kang, E. J. Jeong, J.-I. Park, K.-M. Han, S. Lee, B. W. Yoo, B. W. Koo, J. Y. Kim, W. H. Lee, K. Cho, H. A. Becerril and Z. Bao, *J. Am. Chem. Soc.*, 2009, **131**, 6124.
11 M. Funahashi, *Mater. Chem. Front.*, 2021, **5**, 8265.
12 K. Iakoubovskii and M. Yoshio, *Chem. Commun.*, 2023, **59**, 7443.
13 L.-X. Guo, Y.-B. Xing, M. Wang, Y. Sun, X.-Q. Zhang, B.-P. Lin and H. Yang, *J. Mater. Chem. C*, 2019, **7**, 4828.
14 S. Bujosa, L. Rubert, C. Rotger and B. Soberats, *Commun. Chem.*, 2024, **7**, 296.
15 J. A. Knöller, F. Müller, T. Matulaitis, J. M. dos Santos, A. K. Gupta, E. Zysman-Colman and S. Laschat, *Chem. Sci.*, 2024, **15**, 18022.
16 R. Ahmed, P. K. Behera, A. KN, A. B, A. Patra, S. Kumar, M. A. G. Namboothiry and A. S. Achalkumar, *ChemPhysChem*, 2025, e202400980.
17 R. I. Gearba, D. V. Anokhin and D. A. Ivanov, *Chem. Commun.*, 2025, **61**, 282.
18 C. Dressel, T. Reppe, M. Prehm, M. Brautzsch and C. Tschierske, *Nat. Chem.*, 2014, **6**, 971.
19 C. Dressel, T. Reppe, S. Poppe, M. Prehm, H. Lu, X. Zeng, G. Ungar and C. Tschierske, *Adv. Funct. Mater.*, 2020, **30**, 202004353.
20 T. Reppe, S. Poppe, X. Cai, Y. Cao, F. Liu and C. Tschierske, *Chem. Sci.*, 2020, **11**, 5902.
21 Y. Cao, M. Alaasar, L. Zhang, C. Zhu, C. Tschierske and F. Liu, *J. Am. Chem. Soc.*, 2022, **144**, 6936.
22 O. Kwon, X. Cai, W. Qu, F. Liu, J. Szydlowska, E. Gorecka, M. J. Han, D. K. Yoon, S. Poppe and C. Tschierske, *Adv. Funct. Mater.*, 2021, **31**, 2102271.
23 M. Alaasar, A. F. Darweesh, C. Anders, K. Iakoubovskii and M. Yoshio, *Mater. Adv.*, 2024, **5**, 561.
24 M. Alaasar, Y. Cao, T. Neumann, T. Tan, F. Liu and M. Giese, *Mater. Adv.*, 2024, **5**, 8505.
25 M. Alaasar, S. Poppe, Q. Dong, F. Liu and C. Tschierske, *Angew. Chem., Int. Ed.*, 2017, **56**, 10801.
26 J. Matraszek, D. Pociecha, N. Vaupotič, M. Salamończyk, M. Vogrin and E. Gorecka, *Soft Matter*, 2020, **16**, 3882.
27 M. Alaasar and S. Poppe, *J. Mol. Liq.*, 2022, **351**, 118613.
28 M. Alaasar, X. Cai, Y. Cao and F. Liu, *New J. Chem.*, 2022, **46**, 15871.
29 M. Alaasar, A. F. Darweesh, Y. Cao, K. Iakoubovskii and M. Yoshio, *J. Mater. Chem. C*, 2024, **12**, 1523.
30 C. Tschierske, *Top. Curr. Chem.*, 2012, **318**, 1.
31 M. Poppe, C. Chen, S. Poppe, C. Kerzig, F. Liu and C. Tschierske, *Adv. Mater.*, 2020, **32**, 2005070.
32 C. Anders, T. Tan, V.-M. Fischer, R. Wang, M. Alaasar, R. Waldecker, Y. Cao, F. Liu and C. Tschierske, *Aggregate*, 2025, **6**, e728.
33 Y. Cao, Y. Zhao, T. Tan, F. Liu and M. Alaasar, *Chem. – Eur. J.*, 2025, **31**, e202403586.
34 J. Uchida, B. Soberats, M. Gupta and T. Kato, *Adv. Mater.*, 2022, **34**, 2109063.
35 Z. Zhang, X. Yang, Y. Zhao, F. Ye and L. Shang, *Adv. Mater.*, 2023, **35**, 2300220.
36 I. Dominguez-Candela, I. Zulkhairi, I. Pintre, N. F. K. Aripin, J. Lora-Garcia, V. Fombuena, M. B. Ros and A. Martinez-Felipe, *J. Mater. Chem. C*, 2022, **10**, 18200.
37 A. Patra, P. K. Behera, A. Shah, D. P. Singh, V. A. Raghunathan, A. A. Sudhakar and S. Kumar, *ACS Appl. Electron. Mater.*, 2024, **6**, 4891.
38 V. Bhat Subraya, D. P. Singh, F. Dubois, V. A. Raghunathan, A. Roy and S. Kumar, *ACS Appl. Electron. Mater.*, 2024, **6**, 8828.
39 V. M. Le Corre, *J. Phys. Chem. Lett.*, 2024, **15**, 10001.
40 D. P. Singh, S. K. Gupta, T. Vimal and R. Manohar, *Phys. Rev. E:Stat., Nonlinear, Soft Matter Phys.*, 2014, **90**, 022501.

 